Title: Caliber of zebrafish touch-sensory axons is dynamic in vivo

Abbreviated title: Somatosensory axon caliber

Authors: Kaitlin Ching[1*], Alvaro Sagasti[1†]

Affiliations: [1] Department of Cell, Molecular, and Developmental Biology, University of California, Los Angeles, Los Angeles, California 90095, USA

*Corresponding author: Kaitlin Ching (kaitlinching@ucla.edu)

[†]Corresponding author: Alvaro Sagasti (sagasti@mcdb.ucla.edu)

number of pages: 36

number of figures: 8, videos: 4

number of words in abstract: 230, intro: 417, discussion: 1665

Conflict of interest: The authors declare no competing financial interests.

Acknowledgements: The studies were supported by National Institutes of Health grant R01AR064582. The content is solely the responsibility of the authors and does not necessarily represent the official views of the National Institutes of Health. We thank Van Savage for valuable discussions and suggestions regarding branch analysis, Melissa Emami for providing the Isl1[ss]:lexA, lexAop:mRuby-caax fish, D'Juan Farmer and the UCLA Broad Stem Cell Research Center Microscopy Core for microscope access, and the UCLA Zebrafish Core Facility for animal care. We thank the Sagasti, Farmer, and Koehler labs for helpful discussion and suggestions.

Abstract

Cell shape is crucial to cell function, particularly in neurons. The cross-sectional diameter, also known as caliber, of axons and dendrites is an important parameter of neuron shape, best appreciated for its influence on the speed of action potential propagation. Many studies of axon caliber focus on cell-wide regulation and assume that caliber is static. Here, we have characterized local variation and dynamics of axon caliber in vivo using the peripheral axons of zebrafish touch-sensing neurons at embryonic stages, prior to sex determination. To obtain absolute measurements of caliber in vivo, we paired sparse membrane labeling with super-resolution microscopy of neurons in live fish. We observed that axon segments had varicose or "pearled" morphologies, and thus vary in caliber along their length, consistent with reports from mammalian systems. Sister axon segments originating from the most proximal branch point in the axon arbor had average calibers that were uncorrelated with each other. Axon caliber also tapered across the branch point. Varicosities and caliber, overall, were dynamic on the timescale of minutes, and dynamicity changed over the course of development. By measuring the caliber of axons adjacent to dividing epithelial cells, we found that skin cell division is one aspect of the cellular microenvironment that may drive local differences and dynamics in axon caliber. Our findings support the possibility that spatial and temporal variation in axon caliber could significantly influence neuronal physiology.

Significance Statement

Axon caliber directly influences how quickly neurons send messages to other cells and likely plays a role in neurons' overall health. In the peripheral nervous system, where neurons cover particularly long distances, cell shape can determine whether an animal successfully executes behaviors such as escape responses. We found that axon caliber can vary between locations within the same cell and is highly dynamic. Taking these variations into account may allow neuroscientists to better estimate transmission speeds for cells in neural circuits. We observed

that axon caliber is distorted when nearby skin cells change shape. Thus, cells not classically considered part of the nervous system can also contribute to caliber dynamics, broadening our view of axon caliber determinants.

Introduction

The shape of a neuron's axons or dendrites is central to its function. A key characteristic of axon and dendrite shape is their cross-sectional diameter, also known as caliber. Axon caliber intrinsically influences the speed of action potential propagation (Kriz et al., 2000; Sakaguchi et al., 1993) and may also play a role in cell health and structural stability (Dollé et al., 2018; Perge et al., 2012).

Rohon-Beard (RB) neurons are a type of touch-sensing neuron that develops in early embryonic zebrafish and project skin-innervating peripheral arbors with branched architecture (Fig 1A) (Katz et al., 2021; Shorey et al., 2021; Wang et al., 2013). RB peripheral arbors are afferent axons that detect somatosensory stimuli in the skin and relay messages to interneurons via central axons in the spinal cord, thus promoting behavioral responses.

The significance of axon caliber in cell function has been described for about a century (Hursh, 1939), and it is widely regarded as a cell-wide, static trait despite reports of variations in axon or dendrite caliber over space and time. Axon caliber can vary along the length of axons due to inherent biophysical properties (Griswold et al., 2024), myelination (Seidl, 2014), and mechanical insult (Pan et al., 2024). Dendrite caliber is also known to taper across branch points (Craig and Banker, 1994). Axon caliber has been observed to change over development (Bomont, 2021; Seidl and Rubel, 2016), aging (Metzner et al., 2022), and in response to target size (Voyvodic, 1989a, 1989b) or activity (Nabel et al., 2024; Sinclair et al., 2017). These studies of caliber changes have primarily focused on changes to axon caliber over many days and assume that caliber undergoes little to no change on the timescale of hours. However, the cytoskeletal structures (Costa et al., 2020; Taylor et al., 2012; Wang et al., 2020) and cargoes

79 (Costa et al., 2020; Greenberg et al., 1990; Wang et al., 2020) that can impact axon caliber are
80 dynamic on the timescale of seconds to minutes, prompting us to ask how axon caliber and
81 morphology change on shorter timescales.
82 Here, we characterized axon caliber in zebrafish RB neurons. We found that each single
83 arbor, in vivo, can have a variety of axon calibers, varying within a segment and between sister
84 segments. Axon calibers were dynamic on the timescale of minutes, and these dynamics
85 changed over the developmental timescale of days. Finally, we found that the behavior of
86 epithelial cells in the skin impacts sensory axon caliber, highlighting the complexities of the in
87 vivo axon environment.
88
89 **Materials and Methods**
90 *Fish care*
91 Zebrafish (Danio rerio) adults were housed at 28.5°C with 13.5/10.5-hour light/dark cycles.
92 Embryos were raised at 28.5°C in water containing 0.06 g/L Instant Ocean salt mix (Spectrum
93 Brands, AA1-160P) and 0.05% methylene blue (ThermoFisher, 042771.AP).
94
95 *Injection for sparse labeling*
96 To sparsely label RB neurons for observation of development and axon caliber, adult fish
97 expressing Isl1[ss]:Gal4, UAS:dsRed (Sagasti et al., 2005) were crossed, and resulting embryos
98 were allowed to develop for approximately one hour after fertilization. When embryos reached
99 the 4-cell or 8-cell stage, a single cell in each embryo was injected with approximately 1-3 nL of
100 plasmid containing the Gal4 effector, UAS:egfp-caax, diluted to 10-15 ng/μL in water, with or
101 without phenol red (Sigma, P4758). After injection, embryos were raised as described above.
102
103 *Mounting embryos for microscopy*

104 Unless otherwise indicated, embryos were immobilized on coverslips in 1.2% low-melt agarose
105 dissolved in water (Fisher, BP165-25) and mounted with an equal volume of water containing
106 0.12 g/L Instant Ocean (Spectrum Brands, AA1-160P) and 0.4 mg/mL tricaine (MS-222,
107 Western Chemical Inc.).
108
109 *Developmental time lapse imaging*
110 Embryos injected for sparse labeling were sorted at approximately 20 hours post-fertilization
111 (hpf) to find animals with a single cell expressing EGFP-CAAX in the tail. Selected embryos
112 were immediately dechorionated using forceps and anesthetized in approximately 0.2 mg/mL
113 tricaine (MS-222, Western Chemical Inc.). Embryos were mounted as described above. A cut
114 was made in the agarose posterior to the tail using a fly pin probe to allow room for growth.
115 Embryos were imaged at 5-minute intervals on a ZEISS laser scanning microscope (LSM) 800
116 with a stage heater at 28°C. Magnification was increased as needed by changing objectives to
117 see branching. The most proximal branch point at approximately 28 hpf was identified and
118 visually tracked back to the point of formation within the time lapse for scoring.
119
120 *Line scan and symmetry analysis*
121 Embryos were injected for sparse labeling, as described above. Embryos with a distinct EGFP-
122 CAAX-positive neuron in the tail were dechorionated using forceps and anesthetized in
123 approximately 0.2 mg/mL tricaine (MS-222, Western Chemical Inc.). For this experiment,
124 embryos were immobilized in 1.1 – 1.2% low-melt agarose on No.1 coverslips (Epredia,
125 12460S) to improve available working distance, and water used in initial anesthetization was
126 added before sealing with a glass slide. The primary axon segment was identified as the one
127 that exited the spinal cord and entered the skin. The most proximal branch point was imaged on
128 a ZEISS LSM 880 with Airyscan deconvolution at 27 – 31 hpf. If two neurons or two arbors were
129 present in the same animal or cell, the more posterior one was scored. Line scan analysis was

130 performed using the Line and Plot Profile tools in ImageJ (Schindelin et al., 2012) to find
131 intensity values along a line perpendicular to the center axis of the axon. Axon caliber was
132 measured as the distance between the two peaks on the plot that corresponded to the plasma
133 membrane. For symmetry analysis, axons were measured 3, 4, and 5 μm away from the branch
134 point and averaged to find the caliber of the given segment. The caliber of secondary branches
135 was normalized by dividing by the caliber of the corresponding primary branch. We defined
136 symmetry as S2/S1, which is equivalent to the normalized S2 caliber divided by the normalized
137 S1 caliber.
138
139 *Caliber dynamics time lapse imaging*
140 Embryos were injected for sparse labeling, as described above. Around 24 hpf, embryos were
141 mounted as described above. The proximal region of the axon arbor was imaged on a ZEISS
142 LSM 980, heated to approximately 28°C, and processed with Airyscan Joint Deconvolution at a
143 maximum of five iterations. Time lapses with 5-minute intervals were started at 28 - 31 hpf and
144 acquired until the axon drifted out of the field of view, typically one to two hours. After imaging,
145 embryos were recovered from the mounting agarose using forceps and a probe and grown an
146 additional 24 hours under normal conditions (described above), with the addition of 0.2 mM PTU
147 (1-phenyl 2-thiourea, Sigma, P7629) in the water. At 52 - 55.5 hpf, embryos were mounted and
148 imaged in the same manner as the first day. For scoring, axon segment calibers were measured
149 3 μm from a branch point at every frame of the time lapse, and segments used were each
150 separated by at least one branch point. If the same segments could be identified on the second
151 day, caliber was scored at the same locations for every frame of the time lapse.
152
153 *Dual color time lapse imaging of cell division*
154 To observe axons near dividing cells, transgenic embryos expressing Isl1[ss]:lexA,
155 lexAop:mRuby-caax and tp63:Gal4VP16; UAS:egfp-plcδ-ph (Rasmussen et al., 2015) were

156 mounted as described above and imaged on a ZEISS LSM 980, heated to approximately 28°C,
157 and processed with Airyscan Joint Deconvolution at a maximum of five iterations. Basal skin
158 cells in a rounded state were identified by eye when embryos were 28 - 31 hpf and immediately
159 imaged by time lapse with 5-minute intervals, until daughter basal cells appeared flattened for at
160 least two time points. Axon caliber was measured by line scan analysis, as described above, at
161 1-μm intervals, excluding regions less than 3 μm from a branch point. Border to border length of
162 axons was measured using the Line tool in ImageJ (Schindelin et al., 2012). Orthogonal
163 projections were generated in ZEN Blue (ZEISS).
164
165 *Plotting*
166 All dot plots were created in R. Code can be found at github.com/katieching/CaliberAnalysis.
167 Histograms, dynamics, and pearling plots were created using Microsoft Excel.
168
169 *Experimental design and statistical analysis*
170 For descriptive analyses, an appropriate size for the data set was chosen in advance, and
171 images were collected in experimental batches until the predetermined size was exceeded. For
172 statistical comparisons, a small data set was initially collected, and a power analysis was
173 performed to determine the data set size needed to reach a p-value < 0.05. The data set was
174 collected and analyzed before performing final statistical analyses. Data were excluded as
175 necessary for technical reasons, namely image quality that was too poor for line scan analysis,
176 segments where branch points were closer together than the distance indicated for the
177 experiment (e.g. < 5 μm for symmetry analysis), images in which the primary branch caliber was
178 below the limit of resolution for the system (Fig 3, 4), and axons in which > 20% of
179 measurements at the 1 day post-fertilization (dpf) time point were below the limit of resolution
180 for the system (Fig 5, 6). Significance of differences in paired data was evaluated by paired
181 permutation test in R. Differences between measurements treated as populations were

evaluated by Mann-Whitney test. Analyses performed in R can be found at github.com/katieching/CaliberAnalysis. The sex of animals included in the study was not considered because experiments occurred prior to sex determination.

Results

Rohon-Beard (RB) neurons display a variety of calibers.

RB neurons are touch-sensing neurons that differentiate and become functional within two days of development in embryonic zebrafish and other anamniotes (Katz et al., 2021). The peripheral axons of RB neurons can be identified by transmission electron microscopy (TEM) as membrane-bound ovals between the outermost (periderm) skin cells and lower (basal) skin cells in cross section (O'Brien et al., 2012). Using existing TEM data sets (Faas et al., 2012; O'Brien et al., 2012), we identified peripheral axons of RB neurons and trigeminal neurons, closely-related sensory neurons that perform the same touch-sensing function in the head. By measuring the short axis of these axon cross-sections, we found that calibers ranged from approximately 0.084 to 1.459 μm. This wide range prompted us to ask if axon caliber varies within each cell or only between cells, perhaps by sensory subtype (Gau et al., 2013; Palanca et al., 2013; Tuttle et al., 2024).

To determine if axon caliber can vary within an axon arbor, we sought to measure caliber at consistent locations across many intact cells. To enable absolute measurements of axon caliber, we developed an imaging protocol that paired sparse labeling with super-resolution microscopy. Using transient transgenesis, we generated embryos that expressed a membrane-localized fluorescent protein (EGFP-CAAX) in a single RB neuron in the tail (Fig 1B). We performed time lapse confocal microscopy starting shortly after RB neuron differentiation (20 hours post-fertilization, hpf) and confirmed that branches of the peripheral axon arbor form by growth cone bifurcation as well as collateral sprouting (Haynes et al., 2022; Sagasti et al., 2005), resulting in a highly branched axon arbor within hours of skin entry. To identify a

consistent area of measurement, we observed the most proximal branch point in the peripheral arbor at 27 - 30 hpf and found that it typically forms by collateral sprouting (10 out of 10 cells, Fig 1C-C', Video 1). In these images, some branches of each arbor appeared to be thick while others appeared to be thin (Fig 1D). This observation suggested that axon caliber can vary within each cell and supports the use of this location and technique for studying axon caliber variation.

Caliber varies along the length of an axon segment.

Previous studies have shown that axons are not cylindrical but vary in caliber along their lengths (Bar-Ziv et al., 1999; Greenberg et al., 1990; Griswold et al., 2024; Pullarkat et al., 2006). This phenomenon is sometimes referred to as pearling or varicose morphology. To determine if pearling is observed in live animals, we labeled individual RB neurons and measured axon caliber at 1-μm increments along the length of a segment, shortly after arbor formation began (29 hpf, Fig 2A-B). Variations in axon caliber were visible along the length of all resolvable axon segments, as has been described in mammalian neurons (Greenberg et al., 1990; Griswold et al., 2024). In some instances, axons had distinct pearls (Fig 2A') and in others, more subtle thick and thin stretches without distinct inflection points (Fig 2C). These observations of lengthwise caliber variation confirm that fish and mammalian neurons share similarities in local axon morphology in vivo.

S*ister axon branch calibers are largely uncorrelated with each other.*

Next, we asked how axon caliber varies between different axon segments within a single cell. We labeled individual RB neurons and measured axon caliber near the branch point most proximal to the cell body in 27 - 31 hpf embryos (Fig 3A). The axon segment coming from the spinal cord was designated the primary axon (P), and the axon segments distal to the branch point were designated secondary axons (sister branches designated S1 and S2, for the thicker

234 and thinner segments, respectively). Each segment was measured at three locations (3, 4, and
235 5 μm from the branchpoint), which were averaged to estimate the caliber of that axon segment.
236 By measuring these locations, we observed that axon segments of different calibers exist within
237 the same RB neuron and that secondary branches were typically thinner than the primary
238 branch from which they arose (Fig 3B, P = 0.43 μm, S1 = 0.32 μm, S2 = 0.20 μm). These data
239 confirmed that the average caliber of axons is not uniform across the cell.

240 Because sister segments, S1 and S2, often have different calibers, we sought to assess
241 the relationship between them. We considered two hypotheses: 1) despite variations, each
242 neuron has characteristically thick or thin calibers, and thus S1 and S2 have positively
243 correlated calibers, or 2) S1 and S2 compete for cellular material, and thus their calibers are
244 negatively correlated. To distinguish between these two hypotheses, we compared the S1 and
245 S2 caliber for each neuron. Direct comparison showed a weak relationship between S1 and S2
246 caliber (Fig 3C, R^2 = 0.13). This weak correlation suggests that neither hypothesis is strongly
247 supported.

248 In keeping with this interpretation, symmetry across the branch point was weakly
249 correlated with normalized S1 caliber (Fig 3D, R^2 = 0.04), which we would expect to be strongly
250 correlated if branches compete for cellular material to increase caliber. On the other hand,
251 symmetry is more strongly correlated with normalized S2 caliber (Fig 3E, R^2 = 0.54), suggesting
252 that symmetry is achieved by the thinner branch being thicker, unrelated to the caliber of the S1
253 branch.

254

255 *RB axons taper.*

256 For an RB neuron to function properly, the cell needs electrical signals to travel
257 efficiently. At the time points measured in Fig 3, the arbor was just a few hours old, functional,
258 and continuing to expand. Already, optimal RB neuron function of transmitting sensory signals
259 from the periphery requires efficient propagation of electrical signals from distal to proximal axon

segments (toward the soma). Although the peripheral arbor of RB neurons transmits these afferent signals, as dendrites typically do, we refer to the peripheral arbor as an axon due to its uniformly plus-end-out microtubule organization (Shorey et al., 2021). Tapering is often considered a characteristic unique to dendrites (Craig and Banker, 1994; Jan and Jan, 2010), though more recent analyses suggest that branched axons may taper as well (Desai-Chowdhry et al., 2022).

To facilitate comparison of RB axon branching to other systems, we assessed tapering. First, we calculated the cross-sectional area of each primary and secondary branch ($area = \pi * (\frac{1}{2} caliber)^2$). We compared the primary cross-sectional area to the sum of the secondary cross-sectional areas (Fig 4A). On average, the ratio of the combined secondary cross-sectional areas to the primary cross-sectional area was less than 1 (mean of $\frac{area_{S1} + area_{S2}}{area_P} = 0.888$, Fig 4B), meaning that the RB peripheral arbor tapers in area.

Tapering can influence the health and function of a neuron in many ways, some of which scale with area, and some of which scale with radius (Craig and Banker, 1994; Desai-Chowdhry et al., 2022). Hence, we also compared the radius scaling ratio between secondary branches and their corresponding primary branches ($\frac{r_S}{r_P}$, Fig 4C). The average ratio for the thicker branch was much larger than for the thinner sister branch (mean $\frac{S1}{P} = 0.77 \pm 0.033\, SEM$, and mean $\frac{S2}{P} = 0.49 \pm 0.030\, SEM$, Fig 4D). In evaluating a branched system, some scaling rules hold for the population average, even when branches are asymmetric (Brummer et al., 2017). Hence, to evaluate the function of the arbor more generally, we combined the measurements for the two branches and found that the average ratio (mean $\frac{S}{P} = 0.629 \pm 0.0282\, SEM$) was similar to what is predicted for a system that optimizes for power dissipation rather than time delay (Desai-Chowdhry et al., 2022).

283 Here, we refer to the RB peripheral arbor as an axon due to its plus-end-out microtubule
284 organization (Shorey et al., 2021). Therefore, our observations demonstrate that it is possible
285 for neuronal processes with an axon-like cytoskeletal organization to taper.
286
287 *Axon caliber is highly dynamic.*
288 Having documented variability in axon caliber across locations within each RB neuron,
289 we wondered how calibers change with time. To investigate caliber dynamics, we performed
290 time-lapse imaging in the proximal region of the tail-innervating axon arbors at 28 - 31 hpf
291 (Video 2). Axon caliber changed in several qualitatively different ways over time. We
292 categorized these dynamic behaviors into four categories (Video 3): (1) a traveling pearl,
293 instances of bubble-like regions moving along an axon (Fig 5A), (2) focal inflation and deflation,
294 in which a pearl appears and disappears over the course of multiple time points (Fig 5B), (3)
295 segment widening and narrowing, in which an entire segment thickens and thins between time
296 points (Fig 5C), and (4) a constriction point that appears and disappears, sometimes repeatedly
297 (Fig 5D). This variety of dynamic behaviors suggests that several distinct processes likely
298 contribute to axon caliber dynamics.
299 Axon caliber is known to be altered by changes in target cells (Nabel et al., 2024;
300 Sinclair et al., 2017; Voyvodic, 1989a) or myelination (Ciocanel et al., 2020; Seidl, 2014; Walker
301 et al., 2019), but these developmental processes occur on different timescales from the
302 dynamics we observed with intervals of 5 minutes (Fig 5A-D). To assess caliber dynamics
303 quantitatively, we selected several locations within the proximal region of each neuron, each 3
304 μm away from a branch point, and measured axon caliber at that location over the course of
305 imaging (Fig 5E). Axon caliber was highly dynamic (Fig 5F), with standard deviations ranging
306 from 0.045 μm to 0.095 μm, and could vary with a range of up to four-fold at the same location
307 in less than two hours. Hence, axon caliber and local morphology may be more dynamic than
308 has been widely appreciated.

309 Next, we asked if thin or thick axon segments are more dynamic. First, we assessed
310 absolute dynamicity by comparing average caliber to the standard deviation (SD) or
311 measurements observed during the time lapse (Fig 5G). We found that SD and axon caliber
312 correlated positively, suggesting that thicker axons experienced larger or more fluctuations in
313 caliber. A possible caveat for our measurements is that the lower dynamicity could be due to
314 thin axons spending more time below the limit of resolution. To determine if this was the case,
315 we also assessed relative dynamicity. We calculated relative standard deviation (RSD) for each
316 location by dividing the standard deviation by the average caliber across the movie. Comparing
317 dynamicity across segments revealed that caliber and RSD were negatively correlated, meaning
318 that thick axons were less dynamic than thin axons (Fig 5H). If differences in absolute
319 dynamicity were due to resolution limitations, we would expect to see that relative dynamicity of
320 the thinnest axons is also low. Instead, thin axons had high relative dynamicity, indicating that, if
321 anything, we may have underestimated the dynamicity of thin axons. Together, these results
322 suggest that thick axons have more or larger absolute fluctuations in caliber, but the fluctuations
323 experienced by thin axons are more dramatic when compared to their average caliber.
324
325 *Caliber dynamicity changes over development.*
326 Because we observed caliber to be highly dynamic early in the life and function of RB
327 neurons, we sought to determine if caliber continues to be dynamic later in development. To do
328 this, we recovered embryos after imaging at 28 - 31 hpf and allowed them to continue
329 developing for an additional 24 hours. These fish were re-mounted at 52 - 55.5 hpf and imaged
330 by time-lapse microscopy again. Although all cells had changed shape and axon arbors had
331 grown, often the locations imaged on the first day could be identified, imaged, and measured
332 again on the second day (Fig 6A-B). We found that all resolvable axons continued to be
333 dynamic. However, dynamicity measured as %RSD decreased from the first to the second day
334 in most axon segments (10 out of 11 axon segments decreased. Mean %RSD = 28% at 1 dpf

335 and 20% at 2 dpf, p = 0.036, Fig 6C). Because some axon segments got thicker (n = 6 out of
336 11) and some got thinner (n = 5 out of 11), this decline in relative dynamicity is not simply a
337 product of axons becoming universally thicker. Instead, this dynamicity likely reflects
338 developmental changes that occur in the cell and tissue.
339
340 *Cellular microenvironment can impact axon caliber.*
341 Based on the qualitative variety of caliber dynamics we observed on the minutes
342 timescale (Fig 5A-D), we hypothesized that there are multiple contributors to caliber dynamics.
343 Cell-intrinsic effectors that may cause axon caliber to be dynamic on short timescales, such as
344 cargo transport and contraction of the membrane periodic skeleton, have been described by
345 others (Costa et al., 2020; Wang et al., 2020). However, another contributor is the cellular
346 microenvironment. Mechanical force at the soma has been shown to influence axon and
347 dendrite morphology (Pan et al., 2024). We hypothesized that, in RB peripheral axons, caliber
348 changes could be influenced locally, including by contact with surrounding epithelial cells.
349 Because RB axons are embedded in actively developing skin, they are subject to local
350 deformation caused by morphological changes in surrounding epithelial cells. Specifically, RB
351 peripheral axons grow between two epithelial cell layers, the periderm and basal cells, each of
352 which undergoes rapid expansion at these developmental stages (Fig 1A) (O'Brien et al., 2012).
353 To determine if changes to the shape or adhesion of adjacent epithelial cells can impact
354 the caliber of axons, we performed simultaneous time lapse imaging of axons and the
355 underlying basal cells starting at 28 - 31 hpf (Video 4). We imaged basal cells using a marker of
356 lipid microdomains under the control of the ΔNp63 promoter (Rasmussen et al., 2015; Rosa et
357 al., 2023). One of the most dramatic and frequent perturbations to the RB axon environment
358 occurs when basal cells round up for mitosis, during which the lipid reporter clearly highlights
359 rounded cells against the field of surrounding, flat basal cells (Fig 7A). We measured caliber at
360 1-μm intervals along the length of the axon, from a flat neighbor cell, onto the rounded cell, and

361 onto the next flat neighbor cell (Fig 7B). We found that segments of axon on the rounded cell
362 were significantly thicker than segments of the same axon on the non-dividing neighbor cells
363 (caliber = 0.21 μm on rounded cell, 0.16 and 0.14 μm on non-dividing neighbors, p-value =
364 0.025 and 0.00035, respectively, n = 114 measurement locations, N = 4 axons/fish, Fig 7C).
365 This difference contrasts with the two non-dividing neighbor groups, which did not have
366 significantly different calibers, as expected (p-value = 0.059). Although this observation does not
367 distinguish between mechanical or signaling interactions as the driving factor for caliber
368 changes, these data align with a model in which dynamic properties of the dividing cell may
369 impact local axon caliber.
370
371 *Forces from surrounding cells may impact axon morphology.*
372 One reason why axons might be thicker on rounded cells could be due to changes in
373 tension (Griswold et al., 2024; Pan et al., 2024). As a basal cell enters mitosis, it pulls its
374 borders inward, becoming shorter in planar distance, and rounds up, creating a greater vertical
375 distance (Fig 7D). We used images with the clearest orthogonal projections to obtain estimates
376 of how the dimensions of a dividing basal cell differs from its non-dividing neighbors. Using
377 these estimates, we calculated theoretical changes in axon length as the cell rounds up (Fig
378 7E). To simplify these calculations, we assumed that the axon is fixed at the cell borders and
379 runs in a straight path across the basal cell surface. We found that the rounding of basal cells
380 resulted in a shorter axon path during division than when cells were flat (path length when round
381 ≈ 0.78 * path length when flat). Assuming that axons are adhered to the non-dividing

382 neighboring cells, these estimates are consistent with the axon being under lower tension on the
383 rounded cell than on a non-dividing neighbor cell.

384 Based on our observations of rounded cells and our estimates of length changes, we
385 expected that axon caliber would decline as the daughter basal cells flatten. To test this
386 prediction, we performed time-lapse imaging with 5-minute intervals on the rounded cells,
387 including those in Fig 7C, to see if axon caliber changes as the rounded cell divides and flattens
388 into two daughter cells. For each time point, we measured the distance between the two points
389 where the axon crossed the border of the dividing cell or its daughter cells (Fig 8A). The two
390 time points between which the change in length was greatest were selected, and the caliber of
391 the axon on the rounded cell or its daughters was measured at 1-μm increments for those two
392 time points (Fig 8B-C). We paired measurements by location to assess if there was a significant
393 drop in axon caliber between these two time points. Although axon caliber declined from the
394 round to flat time point, on average, this subtle decrease did not reach statistical significance
395 (caliber = 0.28 μm when the basal cell was round and 0.25 μm when the basal cell was flat, p-
396 value = 0.17, n = 54 measurements, N = 7 axons/fish, Fig 8D). This contrasts with the portions
397 of the axon that were on non-dividing neighbor cells, where the difference could have easily
398 occurred by random chance (p-value = 0.94, n = 37 measurements). This result suggests that
399 the decrease in average axon caliber as the underlying basal cell flattened is small and likely
400 not meaningful.

401 Despite the lack of change in average caliber, visual assessment of the videos appeared
402 to show a change in morphology during basal cell flattening (Fig 7A, 8C). Tension and
403 mechanical force may be an important parameter in pearling (Bar-Ziv et al., 1999; Griswold et
404 al., 2024; Pan et al., 2024; Pullarkat et al., 2006), so we wondered if thick regions (i.e. pearls)
405 and thin regions (i.e. connectors) undergo different changes during basal cell division.

406 To assess morphological changes to axons during basal cell division, we calculated
407 pearling as the standard deviation of measurements taken along the length of each axon for the
408 rounded time point and for the flat time point. By pairing values from each movie, we found that
409 one subset of axons became more pearled (increased SD) and the rest became less pearled
410 (decreased SD), resulting in two groups of cellular responses to flattening (Fig 8E). This
411 heterogeneity might suggest that either 1) different responses arise from heterogeneity among
412 the RB neuron population, or 2) our 5-minute intervals do not provide sufficient time resolution
413 to capture cellular responses to tension, which may occur in less than 10 minutes (Sinha et al.,
414 2011; Sitarska and Diz-Muñoz, 2020). Regardless of the reason, these results demonstrate that
415 axon morphology changes with basal cell flattening, though additional complexities remain to be
416 explored.
417
418 **Discussion**
419 *Tapered architecture in branched sensory axons*
420 We have found that the calibers of axon segments in the same RB neuron can be largely
421 independent of one another, highly dynamic, and likely shaped by multiple determinants,
422 including contact with epithelial cells. Variation in axon caliber had previously been observed
423 along short stretches of fixed axons in rodent neurons (Greenberg et al., 1990; Griswold et al.,
424 2024), in response to developmental changes to the neuron's environment and signaling (Bin et
425 al., 2024; Ford et al., 2015; Kumar et al., 2005; Metzner et al., 2022; Nabel et al., 2024;
426 Sánchez et al., 1996; Seidl, 2014; Seidl et al., 2010; Seidl and Rubel, 2016; Sinclair et al.,
427 2017), and with forces on millimeters-length scales (Pan et al., 2024). Our results expand upon
428 these findings by characterizing caliber variations in vivo across a branched axon, with fine
429 timescale, and with local deformations caused by epithelial cell division.
430 The cutaneous axon endings of touch-sensing neurons, including trigeminal, dorsal root
431 ganglion (DRG), and RB neurons, share characteristics with both dendrites and axons. Like

432 dendrites, they detect stimuli from the periphery and relay signals towards the cell body, but, like
433 axons, their microtubules are oriented plus-end-out (Shorey et al., 2021). We found that the
434 branched axon arbors of RB neurons taper across the most proximal branch point, becoming
435 narrower in caliber and cross-sectional area further from the soma (Fig 4). This feature is often
436 regarded as a characteristic of dendrites, not of axons (Craig and Banker, 1994; Jan and Jan,
437 2010). Mechanisms of signal relay from periphery to soma in RB neurons have not been fully
438 elucidated. If RB neurons fire action potentials, then their tapering (Fig 5) would favor afferent
439 action potential conduction, as signals travel from the periphery toward the soma. In measuring
440 the radius scaling ratio, we found it to be consistent with neurons optimized for power
441 dissipation, which aligns well with a more graded, dendrite-like signal transduction (Desai-
442 Chowdhry et al., 2022). Together, our findings are consistent with a model in which tapering
443 may be most aligned with the direction of functional signal propagation rather than microtubule
444 polarity. Whether our findings hold true for other axons, especially afferent axons, remains to be
445 explored.

446 In comparing sister axon branches, we hypothesized that sister branches are related to
447 each other, resulting from either cell-wide effects or a competition for cellular materials. Instead,
448 we found that their calibers are largely uncorrelated with each other, despite being in close
449 proximity and sharing a cytoplasm. Interestingly, we observed varying degrees of symmetry,
450 ranging from pairs of sister branches with the same caliber to highly asymmetrical pairs, where
451 one secondary branch is much thicker than the other. One reasonable hypothesis to explain this
452 observation could be that branches of different symmetry form by different mechanisms. For
453 example, highly asymmetric branches might have formed by collateral sprouting and symmetric
454 branches by growth bifurcation. However, we found a full spectrum of symmetry values, not a
455 bimodal distribution, arguing against this hypothesis (Fig 3D-E). Moreover, though bifurcations
456 are common in RB arbor outgrowth (Haynes et al., 2022) the first branch point often, if not

always, forms as a collateral (Fig 1C). Thus, collateral sprouting can give rise to segments of a variety of calibers within a few hours of formation, highlighting the malleability of axon caliber.

Mechanisms of caliber variation over time and space

We found that caliber dynamicity changed over development (Fig 6). Many developmental changes could account for a shift in dynamicity, including changes within the cell itself, such as cargo transport (Costa et al., 2020; Wang et al., 2020), or changes to the extracellular environment, such as axon ensheathment (Jiang et al., 2019; O'Brien et al., 2012; Rosa et al., 2023). Time lapse imaging of axon caliber also revealed multiple qualitatively different types of dynamics (Fig 5A-D), which we refer to as traveling pearls, focal inflation and deflation, segment widening and narrowing, and constriction points. This variety suggests that there are likely multiple contributors to variations in axon caliber, including both cell-intrinsic and cell-extrinsic mechanisms.

Cell-intrinsic determinants of axon caliber, such as the cytoskeleton, have been studied to varying degrees. One of the best-known caliber determinants is neurofilaments, a type of intermediate filament specific to the nervous system. Increased neurofilament abundance increases axon caliber in mammalian and bird neurons (Elder et al., 1998; Eyer and Peterson, 1994; Kriz et al., 2000; Ohara et al., 1993; Sainio et al., 2021; Sakaguchi et al., 1993; Zhu et al., 1997). Neurofilaments are also highly dynamic. Differences in transport, differential modifications, and dynamics (e.g. folding, severing, annealing) of neurofilaments are all possible ways in which these filaments might contribute to both local regulation and axon caliber dynamics within a cell (Boyer et al., 2022; Çolakoğlu and Brown, 2009; Uchida et al., 2023).

Another cytoskeletal candidate for cell-intrinsic effectors of caliber variation is the more recently discovered membrane periodic skeleton (MPS), regularly-spaced actin rings connected by spectrin tetramers that run the length of axons and dendrites (He et al., 2016; Xu et al., 2013). These rings expand when large cargo such as mitochondria and lysosomes pass

483 through, and altering myosin contractility changes caliber and retrograde trafficking (Costa et al.,
484 2020; Leite et al., 2016; Wang et al., 2020). Observations of cargo transport through the MPS
485 (Costa et al., 2020; Wang et al., 2020), as well as fixed observations that large cargo is often
486 found within pearls (Greenberg et al., 1990), suggest that intracellular cargo transport along
487 microtubules may also contribute to axon caliber dynamics. Work by Griswold et al.
488 demonstrated that myosin contractility can impact pearling (Griswold et al., 2024). Furthermore,
489 the MPS and the propensity of neurons to bead have been found to be protective against low-
490 level mechanical forces (Krieg et al., 2017; Pan et al., 2024), highlighting MPS contractility as
491 another potential source of caliber variations.

492 Other intracellular factors, such as importin beta (Bin 2024), PI3K/AKT signaling (Kumar
493 2005) and membrane composition (Griswold 2024) also regulate axon caliber. Although some of
494 these factors likely influence caliber by regulating the cytoskeleton (Bin 2024), membrane
495 composition is a non-cytoskeletal, cell-intrinsic candidate for causing caliber variation. Griswold
496 et al. found that membrane fluidity can change which size and shape of pearls are most
497 energetically favorable, thereby changing axon morphology (Griswold et al., 2024). Thus, given
498 the dynamic nature of caliber in vivo, changes to membrane composition could also change
499 caliber dynamics.

500 Damage can also influence axon morphology. Markedly pearled or varicose
501 morphologies, sometimes referred to as beading or swelling, often form in damaged axons
502 (Datar et al., 2019; Kerschensteiner et al., 2005; Shao et al., 2020; Williams et al., 2014).
503 Indeed, damaged trigeminal and RB axons, themselves, become dramatically more beaded just
504 before degeneration (Martin et al., 2010). Mechanical forces below the level necessary to break
505 axons have also been found to impact axon and dendrite pearling (Pan et al., 2024). Our
506 observations of variation in caliber in this study were made in anesthetized, healthy embryos
507 and are unlikely to result from axon damage, as neurons remained intact, even after time lapse

508 microscopy. Similarity between these phenomena in healthy and damaged axons may reflect
509 related processes if the healthy malleability of axon caliber is pushed to extremes upon insult.
510 Although much attention has focused on potential intrinsic determinants for axon caliber
511 variation, we considered the possibility that extrinsic influences from surrounding cells might
512 affect axon caliber locally. Cell-extrinsic factors that influence axon caliber include target size
513 (Voyvodic, 1989a) and distance (Seidl et al., 2010), neuronal function (Nabel et al., 2024;
514 Sinclair et al., 2017), and mechanical forces at millimeters-length scale (Pan et al., 2024). Each
515 of these factors likely impacts the entire cell and is, therefore, unlikely to regulate caliber
516 variation locally.
517 Our study focused on smaller deformations that occur on smaller length scales and
518 timescales. Although myelination is thought to influence local axon caliber (Rydmark, 1981;
519 Seidl, 2014; Swärd et al., 1995), questions remain about the direction and specific nature of this
520 intercellular relationship (Bin et al., 2025; Friede, 1972; Sánchez et al., 1996). RB axon arbors
521 are embedded in a developing epidermis, which undergoes growth and morphogenetic
522 changes. RB axons span tens or even hundreds of micrometers in length and branch to cover
523 large areas of the skin. Hence, each segment of an axon contacts different basal cells, which
524 may each impact the local axon caliber independently.
525 Basal cells can undergo many morphological changes to alter the axon's environment.
526 One important change is ensheathment (O'Brien et al., 2012) (Fig 1A), which increases
527 between 1 and 2 dpf (Jiang et al., 2019; Rosa et al., 2023), possibly contributing to differences
528 in dynamicity between these two developmental time points (Fig 6C). The idea that
529 ensheathment may alter axon caliber is further consistent with the observation that myelinated
530 portions of an axon are thicker than the nodes of Ranvier (Rydmark, 1981; Swärd et al., 1995).
531 Another morphological change in basal cells is rounding for division, which we found
532 changes axon caliber and morphology (Fig 7,8). We hypothesize that changes in tension
533 caused by the movement of cells adjacent to axons are candidates for cell-extrinsic regulators

534 of axon caliber. Division events likely vary in frequency throughout embryonic development,
535 which may further contribute to developmental differences in caliber dynamicity (Fig 6C).
536 Additionally, axons may experience end-to-end stretch as embryos lengthen. Finally, although
537 our studies were in embryonic zebrafish, when the environment surrounding these neurons is a
538 rapidly expanding bilayered epidermis, dynamics are unlikely to cease in adulthood, since the
539 stratified epidermis in both fish and mammals is constantly renewing as basal cells differentiate
540 into higher strata. How caliber variations and dynamics differ in this stratified system remains to
541 be explored. In conjunction with findings that myelination influences axon caliber (Ciocanel et
542 al., 2020; Rydmark, 1981; Seidl, 2014; Swärd et al., 1995; Walker et al., 2019), our results
543 support the model that lengthwise variation, local variations in average caliber, and caliber
544 dynamics may be influenced, in part, by the behavior of surrounding cells.
545

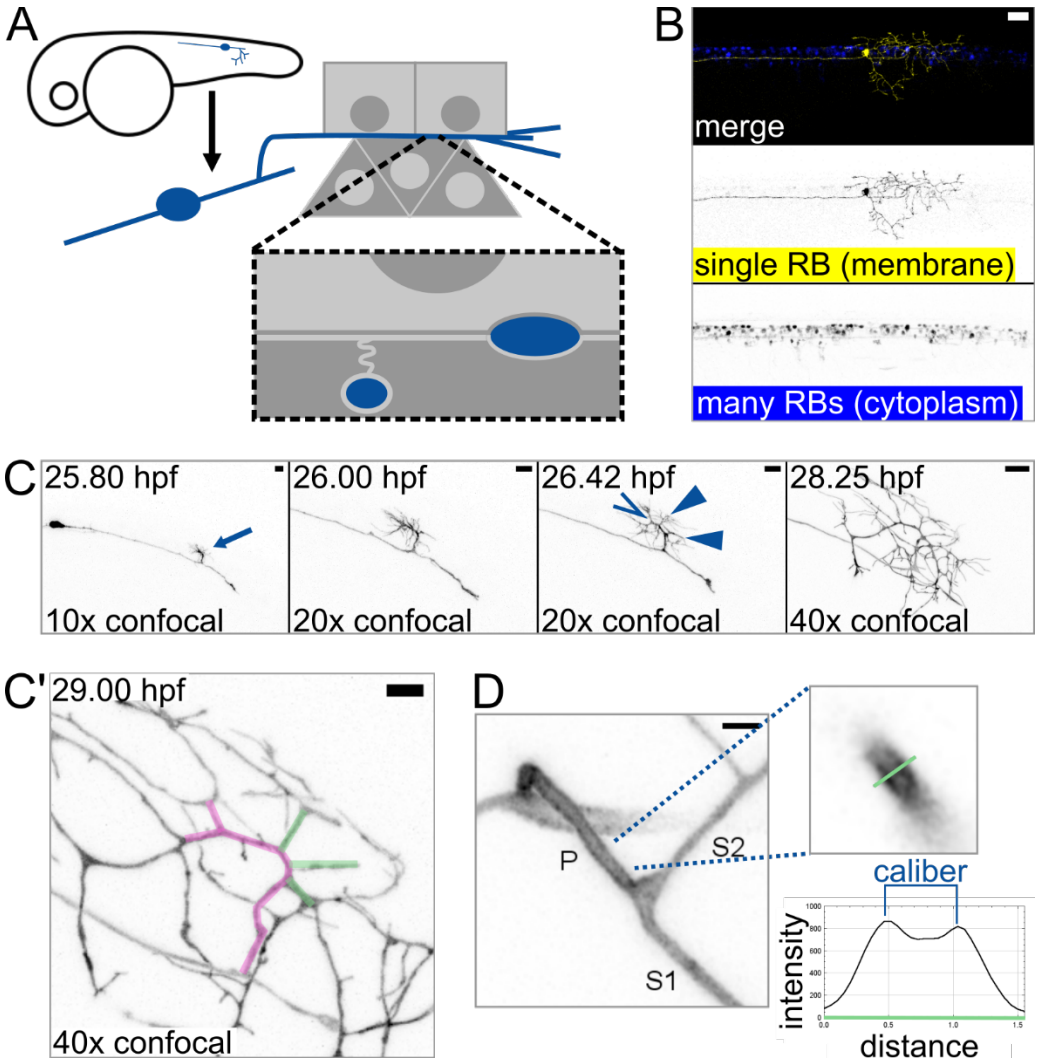

Figure 1: Axon branch development and caliber in sparsely-labeled Rohon-Beard (RB) neurons

(A) Diagram depicting an RB neuron in an embryonic zebrafish. Light grey squares represent periderm (outermost) epithelial cells. Dark grey triangles represent basal epithelial cells, which ensheath some RB axons around 2 - 3 dpf. **(B)** Example of embryonic zebrafish tail with sparse labeling showing one RB neuron expressing EGFP-CAAX among many RB neurons expressing cytoplasmic DsRed. Scale bar: 50 µm. **(C)** Illustrative images taken from time lapse of RB neuron development. Proximal branch point formed by collateral sprouting in 10 out of 10 time lapses. Arrow: formation of main branch in peripheral axon arbor. 26.42 hpf panel shows multiple new branches that formed within minutes of each other. Open arrowhead: growth cone bifurcation event. Solid arrowheads: collateral sprouting events. Scale bars: 10 µm. **(C')** Proximal region of the axon arbor shown in B. Magenta pseudo-colored axon shows the main branch, which branched by growth cone bifurcation. Green pseudo-colored axons show branches that formed by subsequent collateral sprouting. Scale bar: 5 µm. **(D)** Method used for measuring caliber. RB neurons expressing EGFP-CAAX were measured by line scan (green line). Caliber was scored as distance between intensity peaks, as illustrated in example plot. P: primary branch, which extends from spinal cord to skin, S1: thicker secondary branch, S2: thinner secondary branch. Scale bar: 2 µm.

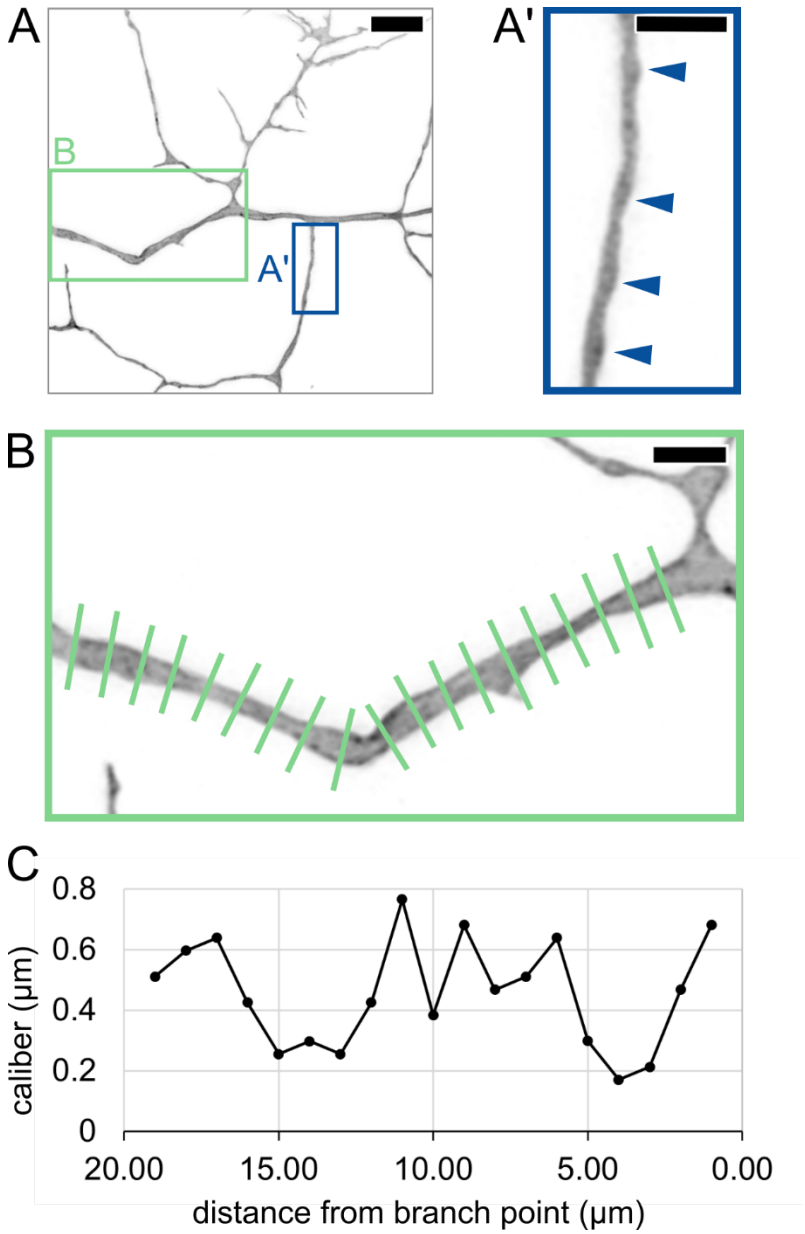

Figure 2: Lengthwise variation in axon caliber
(A) Image of an RB axon arbor at 29.00 hpf. Blue box shows location of inset in A'. Green box shows location of inset in B. Scale bar: 5 µm. **(A')** Inset showing axon branch with pearled morphology. Arrowheads: Thicker regions of axon, resembling "pearls" previously described in mammalian neurons. Scale bar: 2 µm. **(B)** Long axon segment measured by line scan at 1-µm increments. Scale bar: 2 µm. **(C)** Plot of caliber showing variation along the length of axon segment in panel B.

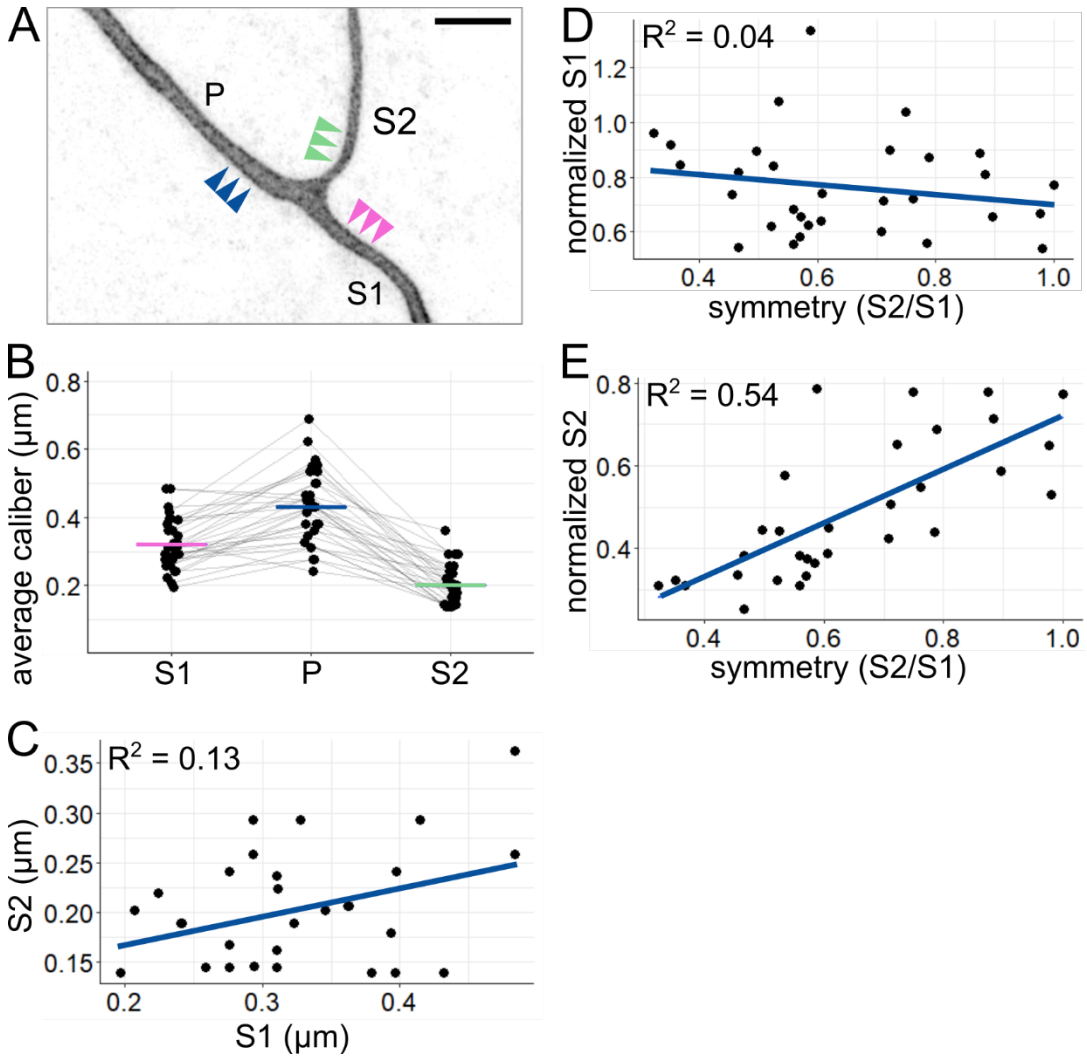

Figure 3: Comparison of axon segments within each arbor
(A) Example image of proximal RB axon arbor. Arrowheads indicate approximate location of line scans for average caliber measurement. P: primary branch, S1: thicker secondary branch, S2: thinner secondary branch. Scale bar: 5 µm. **(B)** Plot of average axon calibers at the proximal branch point. Grey lines connect data points from the same neuron. Horizontal lines: mean values with colors corresponding to branch categories shown in panel A. n = 31 neurons. **(C)** Plot comparing caliber of sister axon segments shown in panel A. **(D)** Plot of branch symmetry versus normalized S1 caliber (S1/P). **(E)** Plot of branch symmetry versus normalized S2 caliber (S2/P). Blue lines in C, D, and E show linear regression.

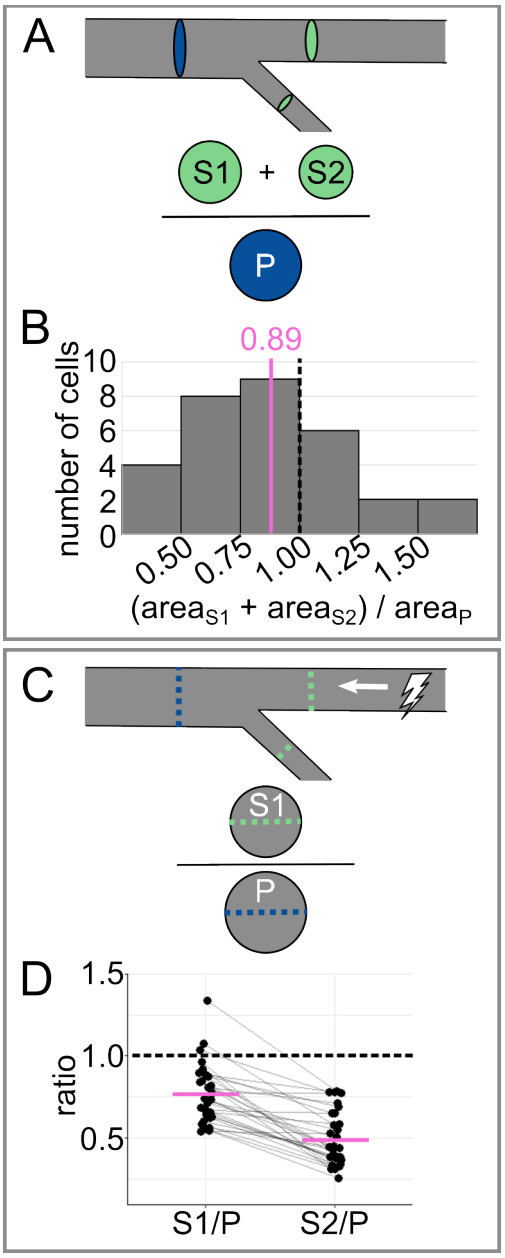

Figure 4: Analysis of tapering across the most proximal branch point
(A) Diagram of tapering analysis in panel B. Combined cross-sectional area of secondaries (S1 and S2) is divided by the cross-sectional area of the primary (P) to evaluate tapering. **(B)** Histogram of cross-sectional area ratios for data shown in Figure 1. **(C)** Diagram of tapering analysis in panel D. Caliber of each secondary (S1 or S2) is divided by the caliber of the primary (P) to estimate the impact of tapering on action potential conduction velocity. **(D)** Plot of caliber ratios for data shown in Figure 1. Grey lines connect data points from the same neuron. In panels B and D, dotted black lines mark reference value 1.0 (no tapering), and magenta lines mark mean values.

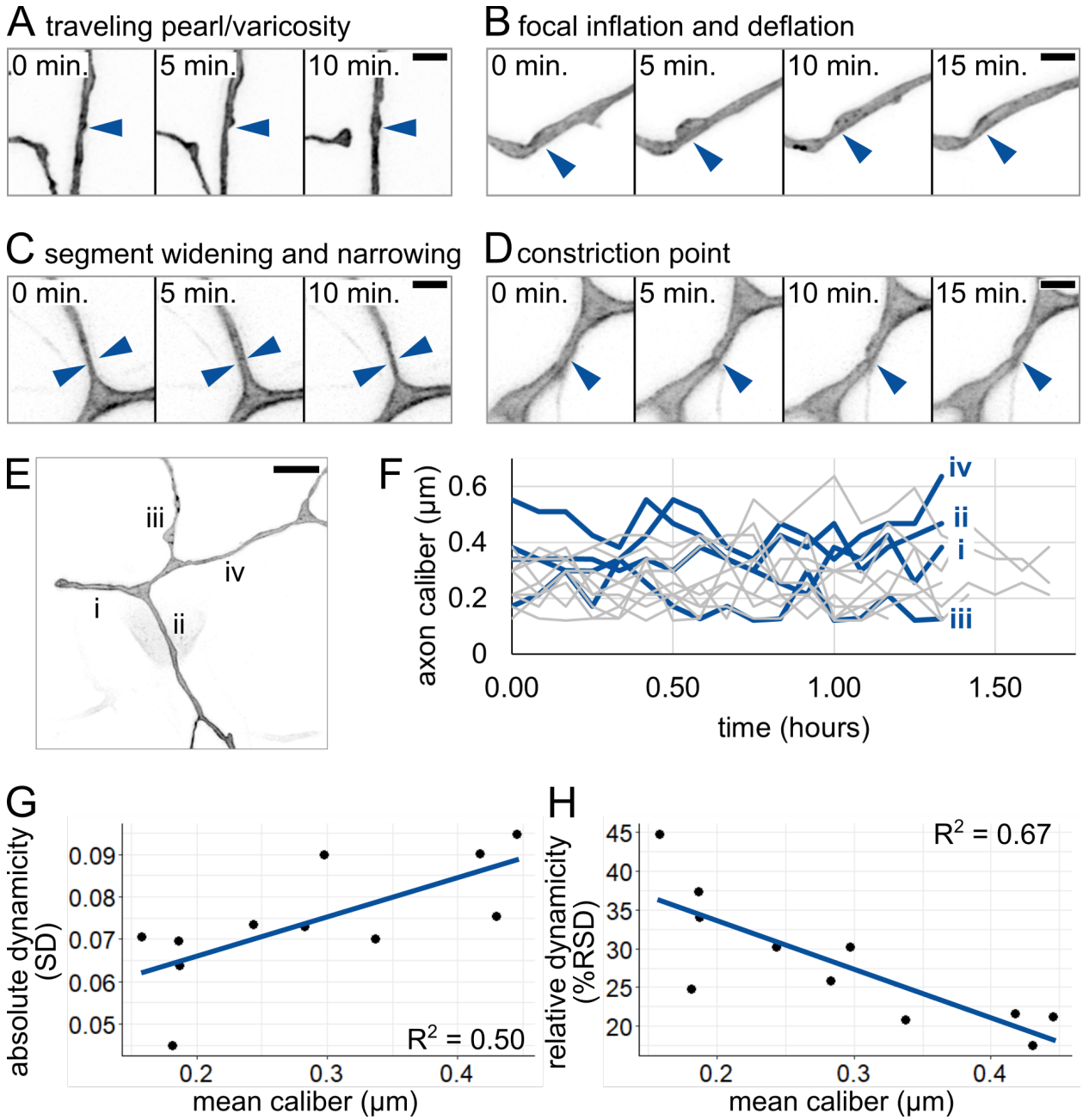

Figure 5: Qualitative and quantitative analysis of caliber dynamics
(A) Example of possible traveling pearl. Short distance traveled allowed for acquisition despite 5-minute intervals. Arrowhead: initial location of pearl. **(B)** Example of focal inflation and deflation event. Puncta containing EGFP-CAAX accumulate during inflation and are seen exiting during deflation. Arrowhead: location of event. **(C)** Example of segment widening and narrowing. Arrowhead pairs denote width at t = 5 minutes. **(D)** Example of constriction point. Arrowhead: location of event. In panels A-D, scale bars: 2 µm. **(E)** Image of axon arbor in the proximal region. Different segments are labeled from proximal to distal: i-iv. Scale bar: 5 µm. **(F)** Plot of axon caliber dynamics, n = 11 axon segments, N = 5 fish. Blue lines: axon segments shown in panel E. Grey lines: all other axon segments measured. **(G)** Plot of mean caliber versus absolute dynamicity (SD) for all axons shown in panel F. Mean caliber is the average at the given location across all time points. **(H)** Plot of mean caliber versus relative dynamicity (%RSD

613 = (SD / mean caliber) * 100) for all axons shown in panel F. In panels G and H, blue lines: linear
614 regression.
615

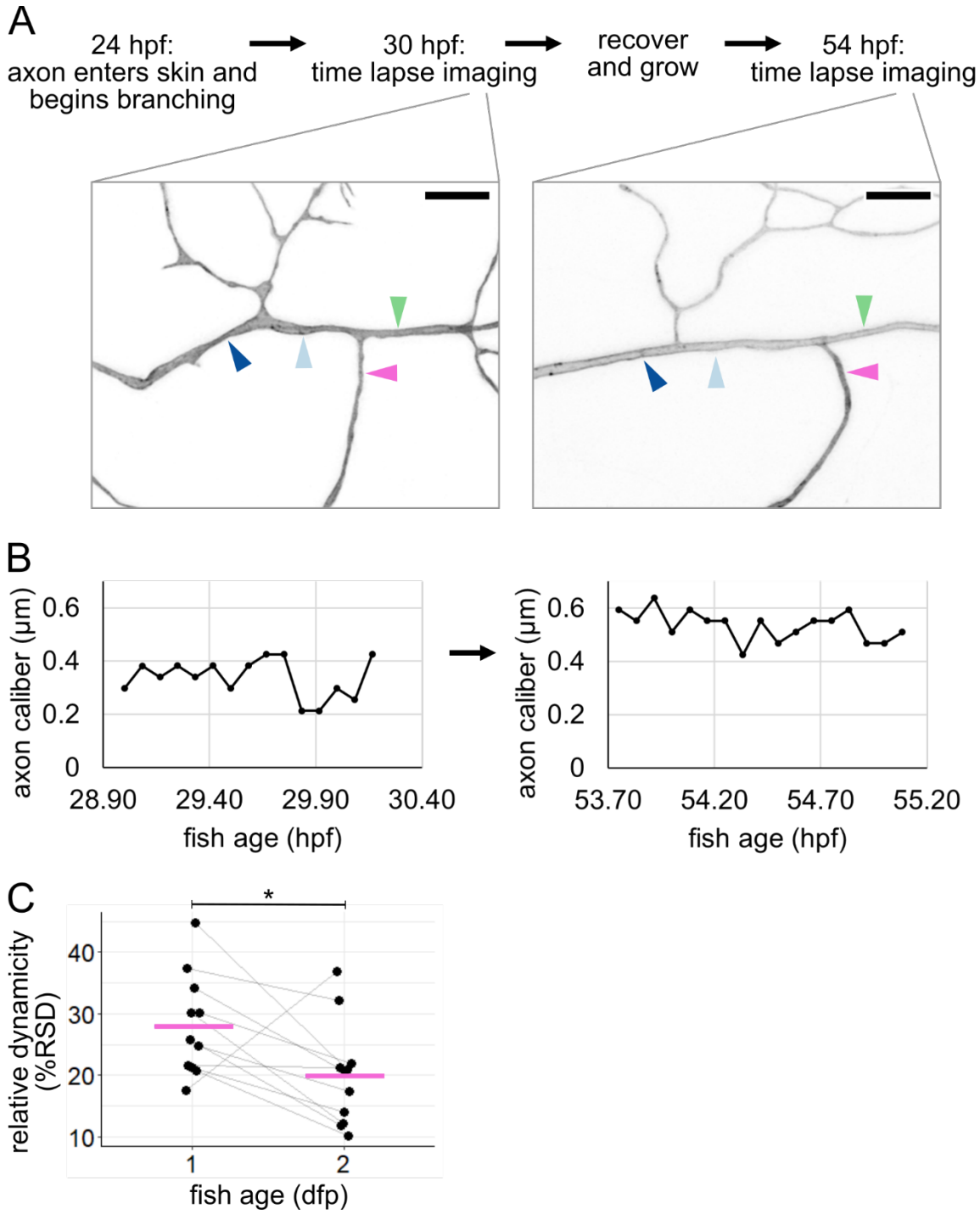

Figure 6: Tracking caliber dynamics over development
(A) Experimental workflow with example images (same neuron as Figure 2). Arrowheads: locations for line scan measurements. Each location is 3 µm from a branch point and separated from other locations by at least one branch point. Scale bars: 5 µm. **(B)** Representative example plots of caliber dynamics for the same segment at 1 dpf and 2 dpf. **(C)** Plot of relative dynamicity (%RSD) at 1 dpf and 2 dpf (same neurons as Figure 5) n = 11 neurons, N = 5 fish. Grey lines connect data points from the same neuron. Magenta lines: mean values. *$p < 0.05$.

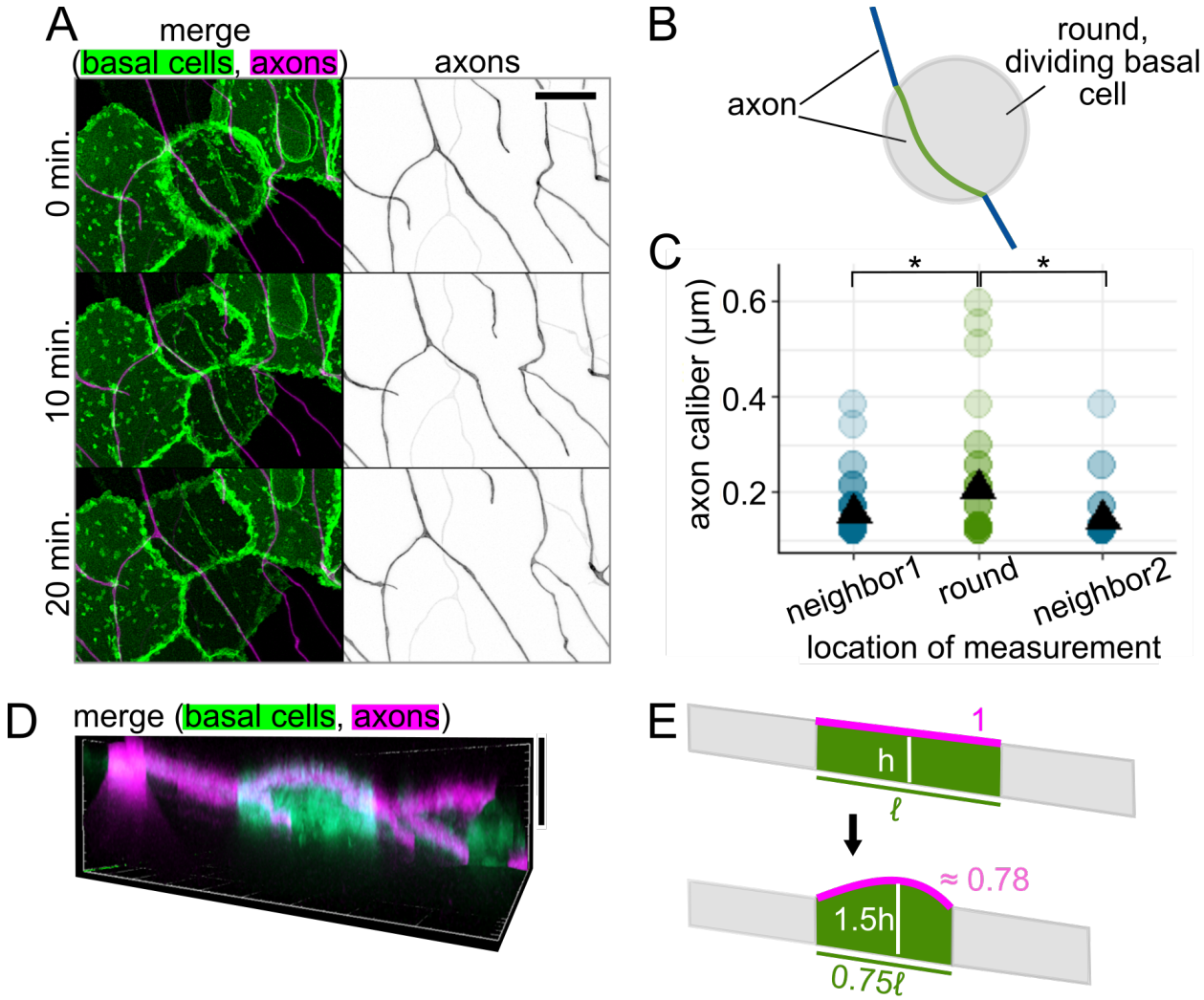

Figure 7: Axon caliber on dividing basal epithelial cells
(A) Representative images of time lapse showing an RB axon adjacent to a dividing basal cell. Basal cells express EGFP-PLCδ-PH. RB neurons express mRuby-CAAX. Scale bar: 10 µm. **(B)** Diagram of an axon on a dividing basal cell that is rounded while undergoing mitosis. Green line: axon segment in contact with dividing basal cell. Blue lines: axon segments on neighboring, non-dividing basal cells. **(C)** Plot of axon caliber measurements grouped by location, n = 114 measurement locations, N = 4 axons/fish. Green dots: caliber of axon on a dividing basal cell. Blue dots: caliber of axon on neighboring cells to one side (neighbor1) or the other (neighbor2) of the dividing basal cell. Black triangles: mean value. *p-val < 0.05. **(D)** Orthogonal projection of a dividing basal cell, which expresses EGFP-PLCδ-PH and is highlighted against non-dividing basal cells due to a variegated expression pattern. An RB axon is in contact with its apical surface, which is rounded upward. Vertical scale bar: 10 µm. **(E)** Diagram comparing axon path length on a rounded, dividing basal cell to its flattened state as an approximation of how basal cell shape changes may impact tension on the axon. Magenta: approximated, theoretical axon length, estimated as the longest distance across the apical surface in an orthogonal projection. Approximate arc length was calculated based on height and length estimates in orthogonal projections. ℓ: original length of basal cell, h: original height of basal cell.

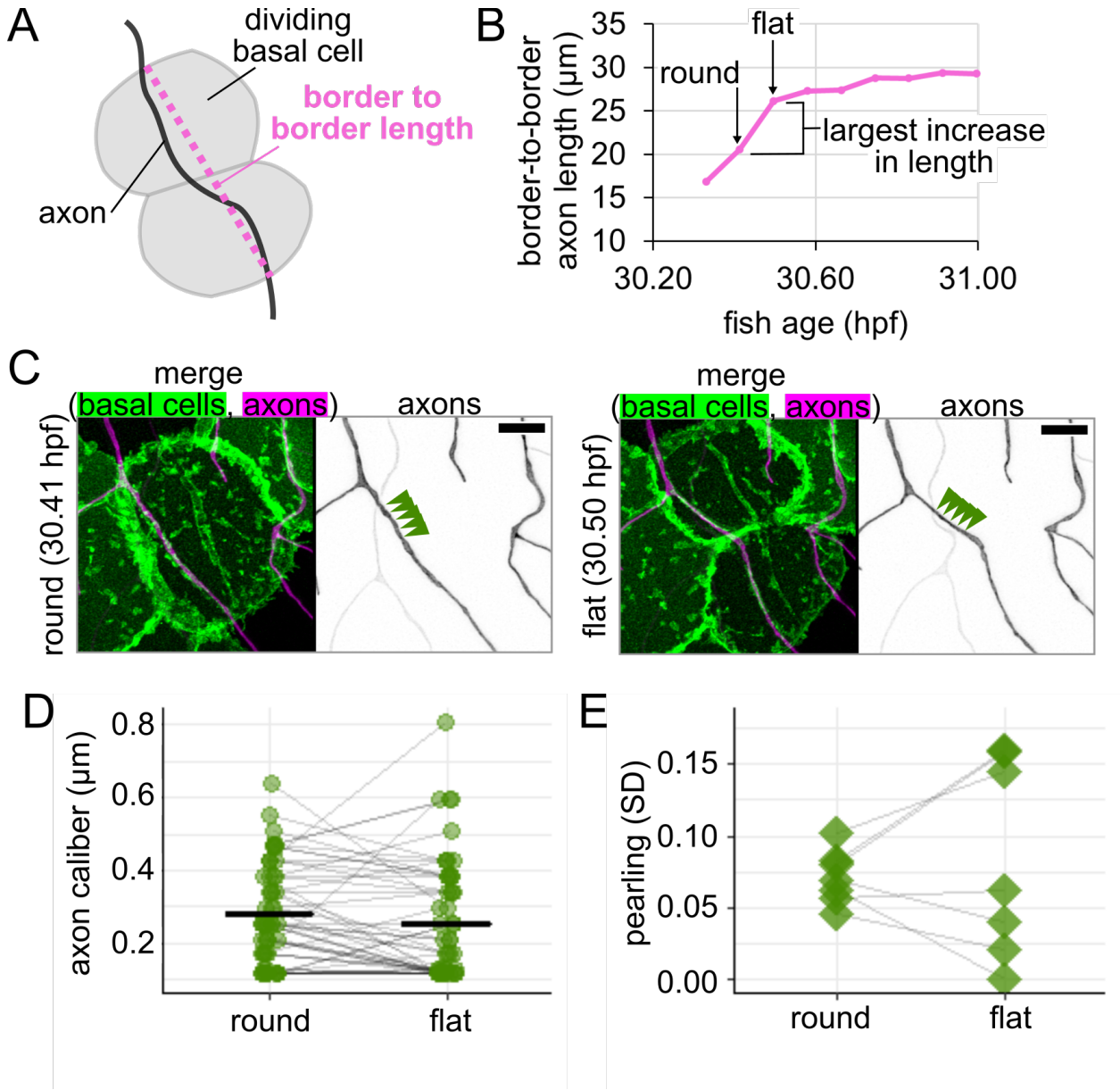

Figure 8: Changes to axon morphology as new basal epithelial cells flatten
(A) Diagram of how border-to-border length was measured for an axon on a dividing basal cell. **(B)** Example plot of changes in border-to-border axon length during time lapse imaging for axon shown in Fig 7A. Round and flat time points are defined as sequential points (5-min. interval) during which border-to-border length increases the most. **(C)** Images from time points highlighted in panel B. Arrowheads: five measurement locations. Scale bars: 5 µm. **(D)** Plot of axon caliber for all locations that remained on the dividing basal cell or its daughter cells, n = 54 measurement locations, N = 7 axons/fish. Grey lines connect data points from the same location. Black lines: mean values. **(E)** Plot of pearling, defined as SD across all locations, to assess morphology change for axons shown in panel D, N = 7 axons/fish. Grey lines connect data points from the same axon.

Video Legends

Video 1: Time-lapse microscopy of axon branch formation in RB neurons.
Confocal time lapse microscopy of RB neuron development in the embryonic zebrafish tail. The main branch of the peripheral axon arbor grows out of the developing spinal cord and into the skin. Shortly thereafter, many branches form by growth cone bifurcation and collateral sprouting. Pseudocoloring in the final frames highlights proximal arbor, and arrows indicate branch points that formed by collateral sprouting events at the times indicated. Scale bars: 5 μm.

Video 2: Time-lapse microscopy of peripheral RB axon.
Super-resolution time-lapse microscopy of the peripheral axon arbor showing the most proximal branch points. Frequent and rapid changes in axon caliber occur within the approximately 1 hour captured prior to drift. Time intervals: 5 minutes. Scale bar: 5 μm.

Video 3: Types of caliber fluctuations in RB axons.
Super-resolution time-lapse microscopy of peripheral axon arbors showing examples of qualitatively different fluctuations in axon caliber. Time intervals: 5 minutes. Scale bars: 2 μm.

Video 4: Time-lapse microscopy of RB axon in contact with mitotic basal keratinocyte.
Super-resolution time-lapse microscopy of an RB axon segment in contact with a skin cell that is undergoing mitosis. Morphological changes in both cells were visualized via membrane fluorescent membrane tags. Magenta: RB neuron labeled with mRuby-caax. Green: Basal keratinocyte labeled with egfp-plcδ-ph. Time interval: 5 minutes. Scale bar: 5 μm.

683 **References**

684 Bar-Ziv R, Tlusty T, Moses E, Safran SA, Bershadsky A (1999) Pearling in cells: a clue to
685 understanding cell shape. Proc Natl Acad Sci U S A 96:10140–10145.
686 Bin JM, Emberley K, Buscham TJ, Eichel-Vogel MA, Doan RA, Steyer AM, Nolan MF, Möbius
687 W, Monk KR, Werner HB, Emery B, Lyons DA (2025) Developmental axon diameter growth
688 of central nervous system axons does not depend on ensheathment or myelination by
689 oligodendrocytes. bioRxivorg.
690 Bin JM, Suminaite D, Benito-Kwiecinski SK, Kegel L, Rubio-Brotons M, Early JJ, Soong D,
691 Livesey MR, Poole RJ, Lyons DA (2024) Importin 13-dependent axon diameter growth
692 regulates conduction speeds along myelinated CNS axons. Nat Commun 15:1790.
693 Bomont P (2021) The dazzling rise of neurofilaments: Physiological functions and roles as
694 biomarkers. Curr Opin Cell Biol 68:181–191.
695 Boyer NP, Julien J-P, Jung P, Brown A (2022) Neurofilament Transport Is Bidirectional In Vivo.
696 eNeuro 9.
697 Brummer AB, Savage VM, Enquist BJ (2017) A general model for metabolic scaling in self-
698 similar asymmetric networks. PLoS Comput Biol 13:e1005394.
699 Ciocanel M-V, Jung P, Brown A (2020) A mechanism for neurofilament transport acceleration
700 through nodes of Ranvier. Mol Biol Cell 31:640–654.
701 Çolakoğlu G, Brown A (2009) Intermediate filaments exchange subunits along their length and
702 elongate by end-to-end annealing. The Journal of Cell Biology.
703 Costa AR, Sousa SC, Pinto-Costa R, Mateus JC, Lopes CD, Costa AC, Rosa D, Machado D,
704 Pajuelo L, Wang X, Zhou F-Q, Pereira AJ, Sampaio P, Rubinstein BY, Mendes Pinto I,
705 Lampe M, Aguiar P, Sousa MM (2020) The membrane periodic skeleton is an actomyosin
706 network that regulates axonal diameter and conduction. Elife 9.
707 Craig AM, Banker G (1994) Neuronal polarity. Annu Rev Neurosci 17:267–310.

708 Datar A, Ameeramja J, Bhat A, Srivastava R, Mishra A, Bernal R, Prost J, Callan-Jones A,
709 Pullarkat PA (2019) The roles of microtubules and membrane tension in axonal beading,
710 retraction, and atrophy. Biophys J 117:880–891.
711 Desai-Chowdhry P, Brummer AB, Savage VM (2022) How axon and dendrite branching are
712 guided by time, energy, and spatial constraints. Sci Rep 12:20810.
713 Dollé J-P, Jaye A, Anderson SA, Ahmadzadeh H, Shenoy VB, Smith DH (2018) Newfound sex
714 differences in axonal structure underlie differential outcomes from in vitro traumatic axonal
715 injury. Exp Neurol 300:121–134.
716 Elder GA, Friedrich VL Jr, Kang C, Bosco P, Gourov A, Tu PH, Zhang B, Lee VM, Lazzarini RA
717 (1998) Requirement of heavy neurofilament subunit in the development of axons with large
718 calibers. J Cell Biol 143:195–205.
719 Eyer J, Peterson A (1994) Neurofilament-deficient axons and perikaryal aggregates in viable
720 transgenic mice expressing a neurofilament-beta-galactosidase fusion protein. Neuron
721 12:389–405.
722 Faas FGA, Avramut MC, van den Berg BM, Mommaas AM, Koster AJ, Ravelli RBG (2012)
723 Virtual nanoscopy: generation of ultra-large high resolution electron microscopy maps. J
724 Cell Biol 198:457–469.
725 Ford MC, Alexandrova O, Cossell L, Stange-Marten A, Sinclair J, Kopp-Scheinpflug C, Pecka
726 M, Attwell D, Grothe B (2015) Tuning of Ranvier node and internode properties in
727 myelinated axons to adjust action potential timing. Nat Commun 6:8073.
728 Friede RL (1972) Control of myelin formation by axon caliber (with a model of the control
729 mechanism). J Comp Neurol 144:233–252.
730 Gau P, Poon J, Ufret-Vincenty C, Snelson CD, Gordon SE, Raible DW, Dhaka A (2013) The
731 zebrafish ortholog of TRPV1 is required for heat-induced locomotion. J Neurosci 33:5249–
732 5260.
733 Greenberg MM, Leitao C, Trogadis J, Stevens JK (1990) Irregular geometries in normal

734 unmyelinated axons: a 3D serial EM analysis. J Neurocytol 19:978–988.
735 Griswold JM, Bonilla-Quintana M, Pepper R, Lee CT, Raychaudhuri S, Ma S, Gan Q, Syed S,
736 Zhu C, Bell M, Suga M, Yamaguchi Y, Chéreau R, Valentin Nägerl U, Knott G, Rangamani
737 P, Watanabe S (2024) Membrane mechanics dictate axonal pearls-on-a-string morphology
738 and function. Nat Neurosci.
739 Haynes EM, Burnett KH, He J, Jean-Pierre MW, Jarzyna M, Eliceiri KW, Huisken J, Halloran
740 MC (2022) KLC4 shapes axon arbors during development and mediates adult behavior.
741 Elife 11.
742 He J, Zhou R, Wu Z, Carrasco MA, Kurshan PT, Farley JE, Simon DJ, Wang G, Han B, Hao J,
743 Heller E, Freeman MR, Shen K, Maniatis T, Tessier-Lavigne M, Zhuang X (2016) Prevalent
744 presence of periodic actin-spectrin-based membrane skeleton in a broad range of neuronal
745 cell types and animal species. Proc Natl Acad Sci U S A 113:6029–6034.
746 Hursh JB (1939) Conduction velocity and diameter of nerve fibers. Am J Physiol 127:131–139.
747 Jan Y-N, Jan LY (2010) Branching out: mechanisms of dendritic arborization. Nat Rev Neurosci
748 11:316–328.
749 Jiang N, Rasmussen JP, Clanton JA, Rosenberg MF, Luedke KP, Cronan MR, Parker ED, Kim
750 H-J, Vaughan JC, Sagasti A, Parrish JZ (2019) A conserved morphogenetic mechanism for
751 epidermal ensheathment of nociceptive sensory neurites. Elife 8.
752 Katz HR, Menelaou E, Hale ME (2021) Morphological and physiological properties of Rohon-
753 Beard neurons along the zebrafish spinal cord. J Comp Neurol 529:1499–1515.
754 Kerschensteiner M, Schwab ME, Lichtman JW, Misgeld T (2005) In vivo imaging of axonal
755 degeneration and regeneration in the injured spinal cord. Nat Med 11:572–577.
756 Krieg M, Stühmer J, Cueva JG, Fetter R, Spilker K, Cremers D, Shen K, Dunn AR, Goodman
757 MB (2017) Genetic defects in β-spectrin and tau sensitize C. elegans axons to movement-
758 induced damage via torque-tension coupling. Elife 6.
759 Kriz J, Zhu Q, Julien JP, Padjen AL (2000) Electrophysiological properties of axons in mice

760 lacking neurofilament subunit genes: disparity between conduction velocity and axon
761 diameter in absence of NF-H. Brain Res 885:32–44.
762 Kumar V, Zhang M-X, Swank MW, Kunz J, Wu G-Y (2005) Regulation of dendritic
763 morphogenesis by Ras-PI3K-Akt-mTOR and Ras-MAPK signaling pathways. J Neurosci
764 25:11288–11299.
765 Leite SC, Sampaio P, Sousa VF, Nogueira-Rodrigues J, Pinto-Costa R, Peters LL, Brites P,
766 Sousa MM (2016) The Actin-Binding Protein α-Adducin Is Required for Maintaining Axon
767 Diameter. Cell Rep 15:490–498.
768 Martin SM, O'Brien GS, Portera-Cailliau C, Sagasti A (2010) Wallerian degeneration of
769 zebrafish trigeminal axons in the skin is required for regeneration and developmental
770 pruning. Development 137:3985–3994.
771 Metzner K, Darawsha O, Wang M, Gaur N, Cheng Y, Rödiger A, Frahm C, Witte OW, Perocchi
772 F, Axer H, Grosskreutz J, Brill MS (2022) Age-dependent increase of cytoskeletal
773 components in sensory axons in human skin. Front Cell Dev Biol 10:965382.
774 Nabel AL, Teich L, Wohlfrom H, Alexandrova O, Heß M, Pecka M, Grothe B (2024)
775 Development of myelination and axon diameter for fast and precise action potential
776 conductance. Glia 72:794–808.
777 O'Brien GS, Rieger S, Wang F, Smolen GA, Gonzalez RE, Buchanan J, Sagasti A (2012)
778 Coordinate development of skin cells and cutaneous sensory axons in zebrafish. J Comp
779 Neurol 520:816–831.
780 Ohara O, Gahara Y, Miyake T, Teraoka H, Kitamura T (1993) Neurofilament deficiency in quail
781 caused by nonsense mutation in neurofilament-L gene. J Cell Biol 121:387–395.
782 Palanca AMS, Lee S-L, Yee LE, Joe-Wong C, Trinh LA, Hiroyasu E, Husain M, Fraser SE,
783 Pellegrini M, Sagasti A (2013) New transgenic reporters identify somatosensory neuron
784 subtypes in larval zebrafish. Dev Neurobiol 73:152–167.
785 Pan X, Hu Y, Lei G, Wei Y, Li J, Luan T, Zhang Y, Chu Y, Feng Y, Zhan W, Zhao C, Meunier

786 FA, Liu Y, Li Y, Wang T (2024) Actomyosin-II protects axons from degeneration induced by
787 mild mechanical stress. J Cell Biol 223.
788 Perge JA, Niven JE, Mugnaini E, Balasubramanian V, Sterling P (2012) Why do axons differ in
789 caliber? J Neurosci 32:626–638.
790 Pullarkat PA, Dommersnes P, Fernández P, Joanny J-F, Ott A (2006) Osmotically driven shape
791 transformations in axons. Phys Rev Lett 96:048104.
792 Rasmussen JP, Sack GS, Martin SM, Sagasti A (2015) Vertebrate epidermal cells are broad-
793 specificity phagocytes that clear sensory axon debris. J Neurosci 35:559–570.
794 Rosa JB, Nassman KY, Sagasti A (2023) Sensory axons induce epithelial lipid microdomain
795 remodeling and determine the distribution of junctions in the epidermis. Mol Biol Cell
796 34:ar5.
797 Rydmark M (1981) Nodal axon diameter correlates linearly with internodal axon diameter in
798 spinal roots of the cat. Neurosci Lett 24:247–250.
799 Sagasti A, Guido MR, Raible DW, Schier AF (2005) Repulsive interactions shape the
800 morphologies and functional arrangement of zebrafish peripheral sensory arbors. Curr Biol
801 15:804–814.
802 Sainio MT, Rasila T, Molchanova SM, Järvilehto J, Torregrosa-Muñumer R, Harjuhaahto S,
803 Pennonen J, Huber N, Herukka S-K, Haapasalo A, Zetterberg H, Taira T, Palmio J, Ylikallio
804 E, Tyynismaa H (2021) Neurofilament Light Regulates Axon Caliber, Synaptic Activity, and
805 Organelle Trafficking in Cultured Human Motor Neurons. Front Cell Dev Biol 9:820105.
806 Sakaguchi T, Okada M, Kitamura T, Kawasaki K (1993) Reduced diameter and conduction
807 velocity of myelinated fibers in the sciatic nerve of a neurofilament-deficient mutant quail.
808 Neurosci Lett 153:65–68.
809 Sánchez I, Hassinger L, Paskevich PA, Shine HD, Nixon RA (1996) Oligodendroglia regulate
810 the regional expansion of axon caliber and local accumulation of neurofilaments during
811 development independently of myelin formation. J Neurosci 16:5095–5105.

812 Schindelin J, Arganda-Carreras I, Frise E, Kaynig V, Longair M, Pietzsch T, Preibisch S,
813 Rueden C, Saalfeld S, Schmid B, Tinevez J-Y, White DJ, Hartenstein V, Eliceiri K,
814 Tomancak P, Cardona A (2012) Fiji: an open-source platform for biological-image analysis.
815 Nat Methods 9:676–682.
816 Seidl AH (2014) Regulation of conduction time along axons. Neuroscience 276:126–134.
817 Seidl AH, Rubel EW (2016) Systematic and differential myelination of axon collaterals in the
818 mammalian auditory brainstem: Systematic and Differential Myelination of Axon Collaterals.
819 Glia 64:487–494.
820 Seidl AH, Rubel EW, Harris DM (2010) Mechanisms for adjusting interaural time differences to
821 achieve binaural coincidence detection. J Neurosci 30:70–80.
822 Shao X, Sørensen MH, Xia X, Fang C, Hui TH, Chang RCC, Chu Z, Lin Y (2020) Beading of
823 injured axons driven by tension- and adhesion-regulated membrane shape instability. J R
824 Soc Interface 17:20200331.
825 Shorey M, Rao K, Stone MC, Mattie FJ, Sagasti A, Rolls MM (2021) Microtubule organization of
826 vertebrate sensory neurons in vivo. Dev Biol.
827 Sinclair JL, Fischl MJ, Alexandrova O, Heβ M, Grothe B, Leibold C, Kopp-Scheinpflug C (2017)
828 Sound-evoked activity influences myelination of brainstem axons in the trapezoid body. J
829 Neurosci 37:8239–8255.
830 Sinha B, Köster D, Ruez R, Gonnord P, Bastiani M, Abankwa D, Stan RV, Butler-Browne G,
831 Vedie B, Johannes L, Morone N, Parton RG, Raposo G, Sens P, Lamaze C, Nassoy P
832 (2011) Cells respond to mechanical stress by rapid disassembly of caveolae. Cell 144:402–
833 413.
834 Sitarska E, Diz-Muñoz A (2020) Pay attention to membrane tension: Mechanobiology of the cell
835 surface. Curr Opin Cell Biol 66:11–18.
836 Swärd C, Berthold CH, Nilsson-Remahl I, Rydmark M (1995) Axonal constriction at Ranvier's
837 node increases during development. Neurosci Lett 190:159–162.

838 Taylor NJ, Wang L, Brown A (2012) Neurofilaments are flexible polymers that often fold and
839 unfold, but they move in a fully extended configuration. Cytoskeleton (Hoboken) 69:535–
840 544.
841 Tuttle AM, Miller LN, Royer LJ, Wen H, Kelly JJ, Calistri NL, Heiser LM, Nechiporuk AV (2024)
842 Single-Cell Analysis of Rohon-Beard Neurons Implicates Fgf Signaling in Axon
843 Maintenance and Cell Survival. J Neurosci 44.
844 Uchida A, Peng J, Brown A (2023) Regulation of neurofilament length and transport by a
845 dynamic cycle of phospho-dependent polymer severing and annealing. Mol Biol Cell
846 34:ar68.
847 Voyvodic JT (1989a) Target size regulates calibre and myelination of sympathetic axons. Nature
848 342:430–433.
849 Voyvodic JT (1989b) Peripheral target regulation of dendritic geometry in the rat superior
850 cervical ganglion. J Neurosci 9:1997–2010.
851 Walker CL, Uchida A, Li Y, Trivedi N, Fenn JD, Monsma PC, Lariviére RC, Julien J-P, Jung P,
852 Brown A (2019) Local acceleration of neurofilament transport at nodes of Ranvier. J
853 Neurosci 39:663–677.
854 Wang F, Julien DP, Sagasti A (2013) Journey to the skin: Somatosensory peripheral axon
855 guidance and morphogenesis. Cell Adh Migr 7:388–394.
856 Wang T, Li W, Martin S, Papadopulos A, Joensuu M, Liu C, Jiang A, Shamsollahi G, Amor R,
857 Lanoue V, Padmanabhan P, Meunier FA (2020) Radial contractility of actomyosin rings
858 facilitates axonal trafficking and structural stability. J Cell Biol 219.
859 Williams PR, Marincu B-N, Sorbara CD, Mahler CF, Schumacher A-M, Griesbeck O,
860 Kerschensteiner M, Misgeld T (2014) A recoverable state of axon injury persists for hours
861 after spinal cord contusion in vivo. Nat Commun 5:5683.
862 Xu K, Zhong G, Zhuang X (2013) Actin, spectrin, and associated proteins form a periodic
863 cytoskeletal structure in axons. Science 339:452–456.

Zhu Q, Couillard-Després S, Julien JP (1997) Delayed maturation of regenerating myelinated axons in mice lacking neurofilaments. Exp Neurol 148:299–316.